ACS OMEGA

Open Access

http://pubs.acs.org/journal/acsodf

Article

Visualization Experimental Investigation on Flow Regulation and Oil Displacement Characteristics of Gel Foam in Fractured-Vuggy Carbonate Reservoirs

Yingda Yang, Gen Rong, Yan Xin, Yongjin Song, and Binfei Li*

Cite This: *ACS Omega* 2024, 9, 40810−40820

Read Online

ACCESS | Metrics & More | Article Recommendations

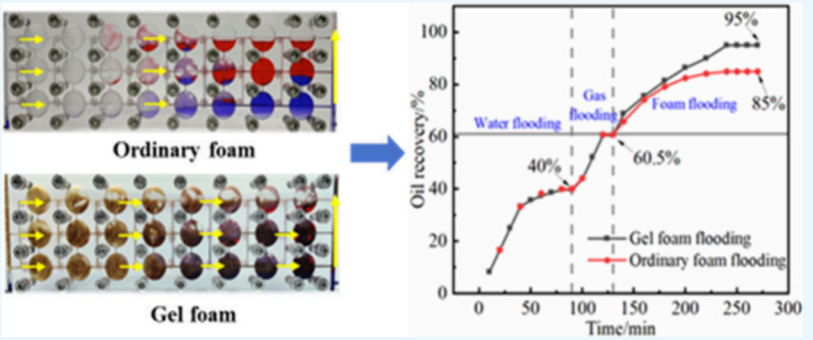

ABSTRACT: Fractured-vuggy reservoirs experience severe channeling during water and gas injection operations, and conventional foam shows weak regeneration capabilities in large-scale fracture spaces, thus failing to effectively seal them. Gel foam combines the advantages of both foam and gel, significantly enhancing the foam's stability and showing good suitability in fractured-vuggy reservoirs. In this article, the plugging and flow regulation properties of gel foam in fractures were studied through fracture displacement experiments. The dynamic plugging capability of gel foam was superior to that of ordinary foam, and its plugging effect was significantly influenced by the fracture opening. Gel foam had strong retention capacity in fractures, and after plugging large-opening fractures, the diversion rate of small-opening fractures was increased by at least 83.3 times during subsequent parallel water flooding, making the flow regulation effect remarkable. Through the oil displacement experiments in typical fractured-vuggy models, the profile control law and enhanced oil recovery performance of gel foam under different fractured-vuggy structures were studied. In the regular fractured-vuggy network, gel foam adhered to occupy the fractured-vuggy space for plugging and controlled the top gas migration direction to synergistically drive the recovery of remaining oil, ultimately achieving a recovery of 95%. In the combination of fractures and irregular vugs, due to the density, gel foam continuously pushed down and right along the fractures to the vugs, pushing the crude oil and formation water in the vugs to migrate to the production well. The recovery of the gel foam flooding stage was as high as 48%, and the final recovery reached 93.5; only a small amount of shielded remaining oil was difficult to drive. The research results are of great significance to the application of gel foam in enhancing oil recovery in fractured-vuggy reservoirs.

1. INTRODUCTION

Fractured-vuggy carbonate reservoirs have attracted strong attention worldwide due to their abundant reserves and high development potential and have gradually become a focal area in oil and gas exploration and development.[1−3] China is an important distribution region of fractured-vuggy carbonate reservoirs in Asia, mainly distributed in Tarim Basin and Ordos Basin, accounting for nearly two-thirds of the proven reserves of carbonate reservoirs in China.[4] Among them, the Ordovician reservoir of Tahe Oilfield in Tarim Basin is the largest fractured-vuggy carbonate reservoir in the world, with crude oil reserves of up to 1 billion tons and an annual output of 9 million tons, demonstrating great development potential.[5,6] However, due to the strong heterogeneity of the fractured-vuggy carbonate reservoir, large karst vugs and structural fractures are the main storage and fluid flow spaces. The permeability and porosity of the carbonate matrix are extremely low, essentially lacking oil storage capacity. This leads to complex interactions between fracture flow, cave flow, and seepage, making the fluid movement very complicated and the exploitation challenging.[7−11]

Received: June 18, 2024
Revised: August 15, 2024
Accepted: September 3, 2024
Published: September 19, 2024

During the development of fractured-vuggy reservoirs, water and gas injections are commonly used to supplement formation energy and enhance oil recovery.[12,13] However, due to the reservoir's physical properties and the effects of gravitational segregation, the injected fluids are highly prone to channeling, leading to significant depletion of formation energy and deteriorating development outcomes.[14,15] Foam has excellent oil−water selectivity and permeability selectivity, and its density can be adjusted to effectively plug channeling pathways and expand the volume affected by the injected fluids, thereby significantly increasing the recovery of fractured-vuggy reservoirs.[16−18] Liu et al.[19] found through the physical experiments of visualized fractured-vuggy model that foam-assisted gas drive can significantly improve the gas drive effect in fractured-vuggy reservoir. The foam effectively plugged gas channeling pathways and expanded the gas drive volume, thus effectively mobilizing bypassed oil and the remaining oil in vugs. Wen et al.[20] found that gas channeling is easy to occur in fractured-vuggy reservoirs, and foam can increase gas migration resistance and control gas mobility, thus effectively improving gas-driven sweep efficiency. Xu et al.[21] found that foam flooding can effectively use the remaining oil that cannot be used by the injected water in the upper fractures and vugs. Additionally, the dynamic plugging caused by foam and the unstable flow field generated by variable foam injection rates further improved the oil recovery.

Due to the harsh reservoir conditions of high temperature and high salinity in fractured-vuggy reservoirs, the foam performance is greatly affected by the reservoir environment. Moreover, the large-scale fractures and vugs have weak shearing effect on the foam, preventing the foam from bursting and regenerating through shearing during transport, which restricts the effective application of foam in fractured-vuggy reservoirs.[22,23] Therefore, developing a highly stable foam system to achieve plugging and displacement control in different spatial locations is crucial for enhancing extraction outcomes.[24,25] Gel foam combines the dual advantages of both foam and gel, possessing the strong plugging properties of gel and resistance ability to high temperature and salinity as well as the high permeability selectivity of foam system. As the gel moves through the channels, it cross-links to block channeling paths, while the gas phase is introduced into the system in the form of small bubbles, reducing density to facilitate reaching deep reservoir areas.[26,27] Song et al.[28] developed a novel dual-cross-linked polymer gel foam system that undergoes a second cross-linking under harsh geological conditions of high temperature and high salinity (140 °C, 24 × 10^4 mg·L^{-1}), further enhancing the stability of the gel foam. Field applications showed that this gel foam significantly controls gas channeling, effectively adjusts gas drive paths, and improves recovery. Li et al.[29] designed a fractured-vuggy carbonate reservoir model to study the impact of gel foam injection speed on recovery and identified the types and mechanisms of drivable residual oil in fractured-vuggy reservoir. Although these studies provide important support for the application of gel foam in fractured reservoirs, research on the plugging regulation law of gel foam between fractures is still lacking, and the characteristics of oil displacement in different multifracture structures need further clarification.

In this study, the plugging and flow regulation performance of gel foam in fractures was studied through fracture displacement experiments. Based on the actual geological data, typical fracture-cavity models were designed to carry out oil displacement experiments, and the regulation and displacement laws of gel foam in different fractured-vuggy structures and the effect of enhancing oil recovery were clarified. This work can provide theoretical support for the application of gel foam in fractured-vuggy reservoirs.

2. EXPERIMENTAL SECTION

2.1. Materials. The simulated formation water used in the experiment was prepared according to the actual ionic composition of the formation water from the Tahe Oilfield, with a mineralization close to 220 000 mg/L. The content of each component is as shown in Table 1. Nitrogen (N_2, 99.9% purity) was provided by Qingdao Xinkexin Gas Co., Ltd. The chemical reagents used to prepare the gel foam include surfactant YF-1, polymer TH-2, and cross-linking agents (catechol and urotropine), all of which were provided by the Northwest Bureau of Sinopec. YF-1 is an anionic−nonionic surfactant with good high temperature and high salinity resistance, which is compounded by an anionic sulfonate surfactant (YM-1) and polyether nonionic surfactant (FM-1). The industrialized temperature-resistant and salt-tolerant polymer TH-2 is copolymerized by acrylamide (AM)−methylpropanesulfonic acid (AMPS) with a relative molecular weight of 6 × 10^6 to 8 × 10^6, and the content of AMPS is 30%.

Table 1. Composition of Formation Water in Tahe Oilfield

material	molar concentration (mmol/L)	molar mass (g/mol)	concentration (mg/L)
NaCl	3110.093	58.5	181940.4
$CaCl_2$	281.8125	111	31281.19
$MgCl_2$	48.41	95	4598.95
Na_2SO_4	1.5625	150	234.375
$NaHCO_3$	0.5547	90	49.923

Preparation of Gel Foam. (1) Surfactant YF-1 (0.7 wt %), polymer TH-2 (0.8 wt %), cross-linker catechol (0.7 wt %), and urotropine (0.7 wt %) were combined in a beaker filled with corresponding mass of simulated formation water, placed on a rotor, and stirred for 6 h on a magnetic stirrer to form the gel foam base liquid. (2) The base liquid was stirred with a high-speed stirrer, and the rotating speed was set at 8000 rpm for 3 min so that the liquid was fully stirred and foamed.

Stability of the Gel Foam. Part of the gel foam was put into a temperature-resistant and pressure-resistant ampule bottle and placed in a high-temperature oven at 130 °C to observe the gel-forming state of the gel foam. The subsequent gelation state of gel foam is shown in Figure 1, and there was no obvious morphological change after being placed at high temperature for 7 days, indicating that gel foam can maintain strong stability after gelation, which can lay a foundation for effective application in high-temperature fractured-vuggy reservoirs.

In order to make the indoor experimental results as close as possible to the real reservoir situation, the simulated oil used in the experiment was prepared by mixing liquid paraffin and kerosene at a 10:1 ratio, and its viscosity is close to that of crude oil under formation conditions. The viscosity−temperature curve of the simulated oil was measured by using an MCR302 Anton Paar rheometer, as illustrated in Figure 2. The simulated oil was dyed with oil red, and the simulated formation water was dyed with bright blue to differentiate the two fluids in the model visually. Both the oil red and bright

https://doi.org/10.1021/acsomega.4c05686
ACS Omega 2024, 9, 40810−40820

Figure 1. Subsequent colloidal state of gel foam at high temperature and high salinity.

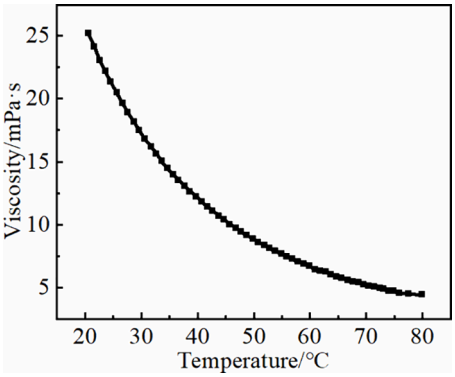

Figure 2. Viscosity−temperature curve of simulated oil.

blue dyes are of analytical grade and were purchased from Macklin Biochemical Co., Ltd.

2.2. Experimental Setup. A micropump (LSP01-2A, flow range 0.0002 μL/min to 8.6699 mL/min, Baoding Lang Hengliu Pump Co., Ltd.) was used to control the injection speed of the fluid. A magnetic stirrer (HJ-6B, speed range 0−1400 rpm, Xicheng Xinrui Instrument Factory) was used for stirring solutions. A balance (PL3002, range 0−3100 g, Shanghai Mettler-Toledo Instruments Co., Ltd.) was used for weighing reagents. A high-speed stirrer (GJ-3S, speed range 0−15000 r/min, Qingdao Haitongda Co., Ltd.) was used for preparing foam. A high-precision pressure sensor (pressure range 0−25 MPa, Haian Petroleum Scientific Research Instrument Co., Ltd.) was used to measure the injection pressure. Additional supporting equipment includes a high-speed camera, computer, an LED lighting panel, syringes, graduated cylinders, and beakers.

2.3. Visualization Models Design. To reasonably simulate the migration and distribution characteristics of fluids in fractures and vugs, various visualization models were designed and fabricated, including a regular single fracture model, a regular fractured-vuggy network model, and a fracture-irregular vugs combination model. All models were made of acrylic (PMMA) material, providing excellent transparency, with a processing precision in the tens of micrometers.

Regular Single Fracture Model. As shown in Figure 3, the model consists of two long acrylic plates. The lower acrylic plate is engraved with four fractures of different openings, and the two acrylic plates are fastened together by multiple rows of screws. The openings of the four fractures from top to bottom are 2, 1, 0.5, and 0.1 mm, respectively. The depth of the fractures is 2 mm, and the overall length of the fractures is 1 m. Screws that can be connected to pipelines are placed at both ends of each fracture, serving as the injection and production ends.

Regular Fractured-Vuggy Network Model. As illustrated in Figure 4, the bottom acrylic plate of the model is engraved to form an entire fractured-vuggy space. The main structure includes three horizontal fractures, nine vertical fractures, and 24 equally sized, regularly arranged circular vugs. These components are sealed with an upper acrylic plate using screws. Each fracture had a depth of 4 mm. The openings of the three horizontal fractures, from top to bottom, are 0.4, 0.8, and 1.2 mm. The vertical fractures are arranged in groups of three, with apertures of 0.4, 0.8, and 1.2 mm, respectively. The circular tubes have a diameter of 25 mm, and the fractures connecting the vertical tubes have an opening of 0.4 mm. The left and right sides feature grooves that serve as the injection and production wells, each with a width and depth of 4 mm. The flow space of the model is 60 mL.

Fractures-Irregular Vugs Combination Model. As shown in Figure 5, the main structure of this model consists of a heterogeneous fracture network interwoven horizontally and vertically, along with four vugs carved based on the actual shapes of vugs in the target formation. This simulates the interconnected situation between heterogeneous fractures and multiple voids in a real formation. The model is secured with screws around its perimeter and at key points. The opening distribution of the fractures is as follows: vertical fractures from left to right are 0.4 mm × 2, 0.8 mm × 2, 0.4 mm × 3, 1.2 mm, 0.4 mm, 0.8 mm, 0.4 mm × 4. Horizontal fractures from top to bottom are 0.8 mm, 0.4 mm × 2, 1.2 mm, 0.4 mm, 0.8 mm, 0.4 mm. The 4 mm feature grooves on both sides of the model

Figure 3. Regular single fracture model: (a) schematic diagram; (b) physical diagram.

https://doi.org/10.1021/acsomega.4c05686
ACS Omega 2024, 9, 40810−40820

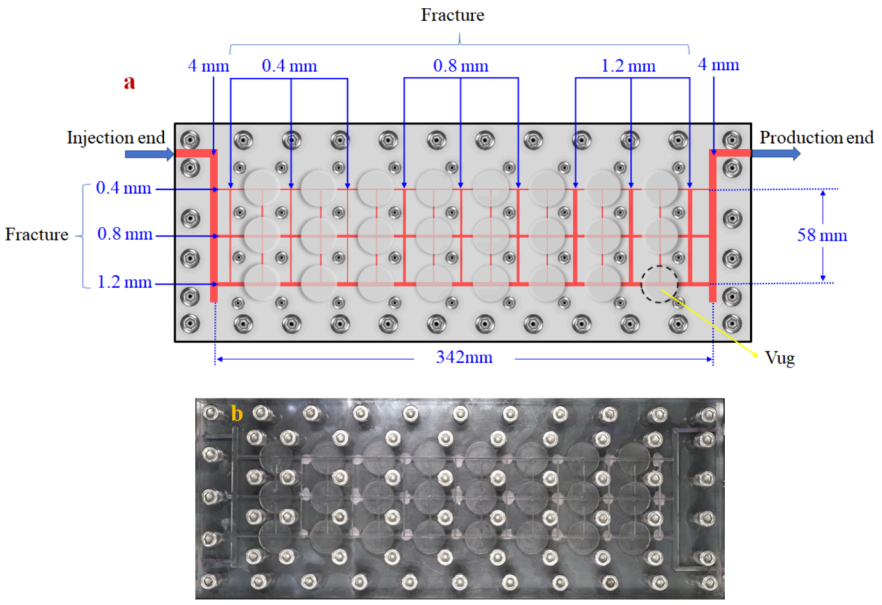

Figure 4. Regular fractured-vuggy network model: (a) schematic diagram; (b) physical diagram.

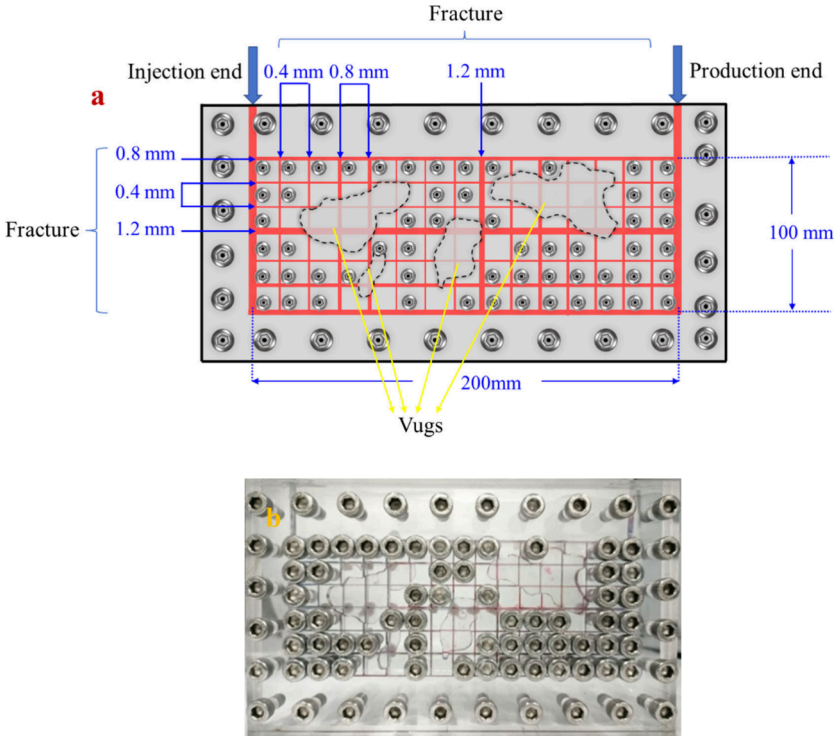

Figure 5. Fractures-irregular vugs combination model: (a) schematic diagram; (b) physical diagram.

serve as the injection and production wells. Each fracture has a depth of 4 mm. The effective flow space of the model is 30.8 mL.

2.4. Plugging and Flow Regulation Experiment in Fractures. Fractured-vuggy reservoirs are prone to water and gas channeling during extraction, resulting in a low oil recovery. This study investigated the plugging and flow regulation performance of gel foam in fractures through displacement experiments. The specific experimental steps are as follows: (1) The fracture model was assembled and checked for airtightness, and the experimental apparatus was connected according to the experimental flowchart shown in Figure 6. (2)

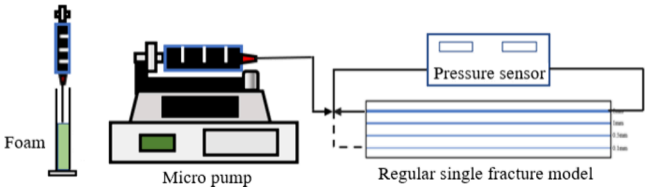

Figure 6. Flowchart of plugging and flow regulation experiment in fracture.

The preprepared foam (ordinary foam, gel foam) was poured into a syringe and injected into the fracture using a

https://doi.org/10.1021/acsomega.4c05686
ACS Omega 2024, 9, 40810−40820

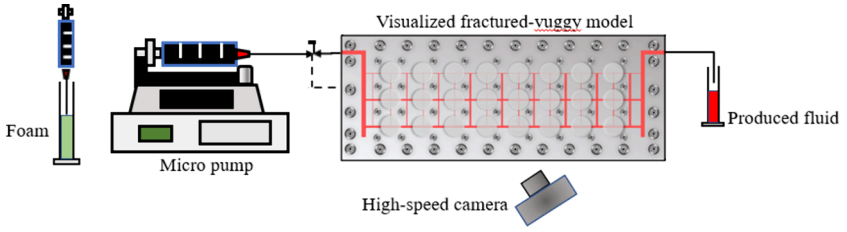

Figure 7. Flowchart of oil displacement experiment in fractured-vuggy model.

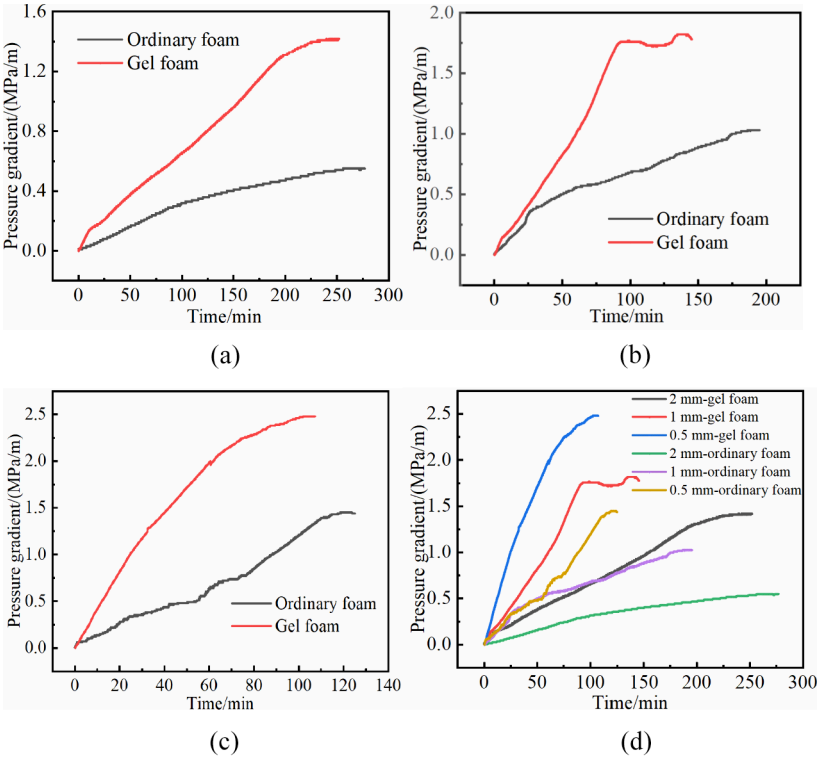

Figure 8. Pressure gradient of foam in fractures with different openings: (a) 2 mm; (b) 1 mm; (c) 0.5 mm; (d) integration.

micropump, with the pressure difference data at both ends of the fracture recorded in real time. (3) The fractures with different opening were replaced, and the above steps were repeated to conduct dynamic plugging tests of the foam in fractures with different openings. (4) The plugging strength of the fracture with an opening of 2 mm was tested, and three-stage continuous displacement experiments of water flooding−foam flooding−water flooding were carried out in turn, and the experiment was ended after the pressure difference stabilized. (5) The diversion experiment was conducted by parallelly connecting two fractures with different openings using pipelines and performing water flooding−foam flooding−water flooding on the parallel fractures, recording the liquid output from both fractures over the same period. The experiment ended when the liquid output from both production ends stabilized and the ratio of the liquid output from each production end to the total liquid output was the corresponding diversion rate. During the experiment, the fracture model was placed horizontally.

2.5. Oil Displacement Experiment in Typical Fractured-Vuggy Models. Oil displacement experiments were conducted using visualization fractured-vuggy models to clarify the effects of different fractured-vuggy structures on fluid distribution and oil recovery under the same injection conditions for water flooding, gas flooding, and different foam systems flooding. The experimental steps are as follows: (1) The model was saturated with simulated oil, and the experimental apparatus was connected according to the flowchart shown in Figure 7. (2) The water flooding, gas flooding, and ordinary foam flooding were conducted on the model. The entire displacement process was recorded using a camera, and the production at each displacement stage was measured using graduated cylinder. (3) The model was cleaned, and gel foam was used to repeat steps 1 and 2. (4) The model with different structure was replaced, and steps 1−3 were repeated for experiments. During the experiment, the fractured-vuggy models were placed vertically.

3. RESULTS AND DISCUSSION

3.1. Plugging and Flow Regulation Performance of Gel Foam in Fractures. *3.1.1. Plugging Characteristics.* Displacement experiments were conducted using ordinary foam and gel foam on fracture models with openings of 0.5 mm, 1 mm, and 2 mm, with fluid flow rate set at 0.5 mL/min. The plugging ability of different types of foam was evaluated by measuring the pressure gradient of the foam in the fractures. The results are shown in Figure 8.

https://doi.org/10.1021/acsomega.4c05686
ACS Omega 2024, 9, 40810−40820

For the same fracture opening, the pressure gradient of gel foam flooding was always greater than that of ordinary foam flooding. In the 2 mm fracture, the flow pressure gradient of gel foam stabilized at 1.41 MPa/m, reaching a stable state after 240 min. The stable pressure gradient of ordinary foam was only 0.55 MPa/m, taking 270 min to stabilize. The final pressure gradient of gel foam was 2.5 times that of ordinary foam, but it reached a stable state in less time. This is due to the better stability of gel foam, resulting in a stronger dynamic plugging ability and higher flow pressure gradient. Ordinary foam is less stable and constantly breaks down and releases liquid during migration, so its dynamic plugging ability is weaker than that of gel foam, requiring more foam fluid to enter the fracture to achieve a stable pressure gradient at the outlet end.

As the fracture opening decreased, the flow pressure gradient of the foam significantly increased. When the fracture opening decreased from 2 to 0.5 mm, the stable pressure gradient of gel foam increased to 2.48 MPa/m and that of ordinary foam increased to 1.45 MPa/m. The pressure gradient of gel foam was reduced to 1.7 times that of ordinary foam. The larger the fracture opening, the stronger is the plugging ability of gel foam compared to ordinary foam. The pressure gradient generated by foam flooding is mainly reflected in the deformation of the foam and the wall effect; therefore, the smaller the opening, the more stable is the foam and the larger is the pressure gradient. Due to its high viscoelasticity, gel foam increases the flow resistance during migration, leading to the Jamin effect superimposition, resulting in a continuously increasing flow resistance. Therefore, it can achieve a high pressure gradient, even in high-aperture fractures, producing an effective dynamic plugging effect.

Further continuous three-stage displacement experiments of water flooding−ordinary foam flooding−water flooding, as well as water flooding−gel foam flooding−water flooding, were conducted on the 2 mm fracture to study the persistence of the plugging effects of the two types of foam.

The change curve of displacement pressure difference in three stages of water flooding−ordinary foam flooding−subsequent water flooding is shown in Figure 9. Initially, the displacement pressure generated by water flooding in the fracture was very low. The pressure difference with ordinary foam reached 0.55 MPa, and in the subsequent water flooding stage, it initially rose to 1.27 MPa but gradually decreased to 0.066 MPa with continued water injection. The stable residual resistance factor was only 3.2. Ordinary foam's plugging ability is weak and not resistant to water injection, failing to effectively plug the fracture. Figure 10 shows the change curve of displacement pressure difference in three stages of water flooding−gel foam flooding−subsequent water flooding. The pressure difference with gel foam reached 1.42 MPa, significantly higher than ordinary foam. In the subsequent water flooding stage, the pressure difference rapidly increased to 3.3 MPa, then slowly decreased and stabilized at 2.69 MPa, with a stable residual resistance factor of 92.8. The pressure difference after gel foam injection was much higher than after ordinary foam injection. This is because gel foam gradually forms gel that adheres to the fracture, requiring higher pressure to break through the foam gel during subsequent water flooding. Additionally, gel foam is highly resistant to erosion and dilution. Even after extensive water flooding, a significant amount of gel foam remains in the fracture, maintaining a high pressure difference. The stability of gel foam, combining the advantages of both foam and gel, is minimally affected by formation water dilution. It can maintain a high residual resistance factor during the injection of high salinity formation water, effectively plugging large-opening fractures.

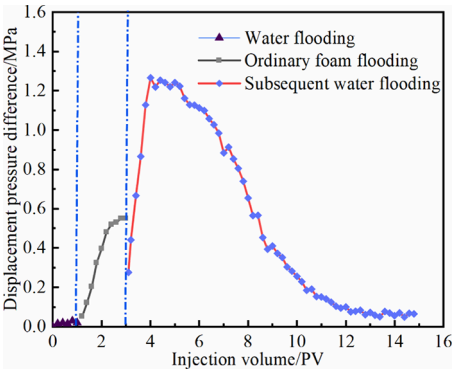

Figure 9. Change curve of displacement pressure difference in water flooding−ordinary foam flooding−subsequent water flooding.

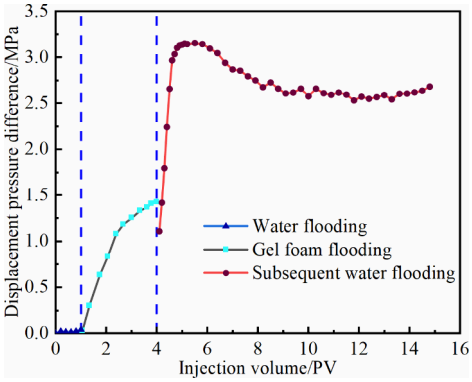

Figure 10. Change curve of displacement pressure difference in water flooding−gel foam flooding−subsequent water flooding.

3.1.2. Flow Regulation Characteristics. Three types of fractures with openings of 2 mm, 1 mm, and 0.5 mm were connected in parallel with fractures with 0.1 mm opening. Diversion experiments using water, ordinary foam, and gel foam were conducted, with the flow rate set at 1 mL/min, to compare the flow regulation capabilities of different types of foam in fractures of varying opening combinations. The proportion of fluid entering the narrow fracture under different fracture combinations is shown in Figure 11.

As can be seen from the figure, there was a significant difference between the diversion rates of water, ordinary foam, and gel foam in the narrow fracture. The diversion rates of gel foam in the 0.1 mm narrow fracture under the three fracture opening combinations were 0.3, 0.49, and 0.78, respectively. For ordinary foam, the diversion rates were 1.53, 2.08, and 2.65, respectively. This is because the viscosity of gel foam is higher than that of ordinary foam and water, making it more likely to flow along a larger opening fracture. The diversion rate in the narrow fracture is smaller and less affected by changes in the opening gradient, which helps maintain the diversion rate in the narrow fracture within a relatively stable range.

Ordinary foam and gel foam were used to plug fractures with openings of 2 mm, 1 mm, and 0.5 mm, which were then

https://doi.org/10.1021/acsomega.4c05686
ACS Omega 2024, 9, 40810−40820

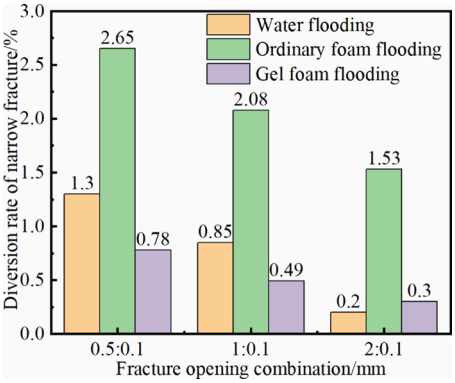

Figure 11. Diversion rates of narrow fractures under different opening combinations.

connected in parallel with 0.1 mm fracture, respectively. The flow regulation effect of subsequent injected fluids was compared after plugging with different foams. The results are shown in Figure 12. Combining Figures 11 and 12, for the

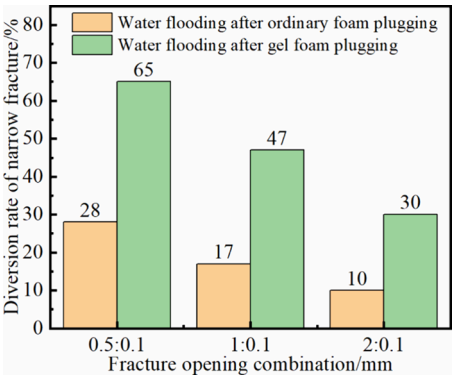

Figure 12. Comparison of the diversion rate of narrow fractures in water flooding after plugging.

three fracture opening combinations, during parallel water flooding, the diversion rate of narrow fracture after foam injection into large opening fracture was much higher than the diversion rate when foam was injected in parallel. After the large opening fracture was plugged with gel foam, the diversion ratio of narrow fracture during parallel water flooding was higher than that after being plugged with ordinary foam in the same opening fractures. During parallel water flooding, the diversion rate of narrow fractures after the large opening fractures plugged with gel foam increased by 100, 95.9, and 83.3 times, respectively, while that of ordinary foam was increased by 10.6, 8.2, and 6.5 times. Ordinary foam has a shorter retention time in fractures, easily breaking down and partially being washed out by subsequent water flooding, leading to partial recovery of fracture permeability. However, ordinary foam initially regulates flow well, allowing a large amount of water to flow through the narrow fractures. Gel foam, on the other hand, retains significantly more in the fractures after plugging, forming a gel that maintains strong plugging for a longer period. Water flooding needs a higher displacement pressure to break through the gel foam plugging. When parallel water flooding is conducted after plugging with gel foam in a large opening fracture, the flow rate in the narrow fracture increases significantly due to the plugging in the large opening fracture by the gel foam. Gel foam provides excellent flow regulation after plugging large opening fracture.[30] Additionally, gel foam has good erosion and dilution resistance, maintaining its plugging effect in large opening fractures and flow regulation effect in narrow fractures even after extensive fluid injection.

3.2. Profile Control and Displacement Performance of Gel Foam in Typical Fractured-Vuggy Model.

3.2.1. Displacement Characteristics in Fractured-Vuggy Network Model. To study the displacement effect of gel foam in a fractured-vuggy reservoir, water flooding, gas flooding, and gel foam flooding were carried out at a fluid flow rate of 0.5 mL/min by using the fractured-vuggy network model.

3.2.1.1. Water Flooding Stage. Figure 13 shows the state of the fractured-vuggy network model after the water flooding stage. In the model, the red liquid is simulated oil, and the blue liquid is simulated water. The left side feature groove serves as the injection well. The right side feature groove serves as the production well. As shown in the figure, water was injected from the left injection well and connected to three fractures of different openings. Due to the effects of gravity and fracture opening, the water preferentially flowed through the large horizontal fracture at the bottom into the vugs, displacing the oil in the bottom region of the model toward the right and out through the production well. Because of the density difference, there was an interface between the water and oil. After all the oil at the bottom of the model was displaced, water flowed upward through the fractures between the vertical vugs, extracting some oil from the middle vugs. However, at this stage, when the produced fluid flowed out through the right production well only containing water, water channeling occurred, and water flooding stopped. At this time, a large amount of remaining oil was left in the upper part of the model.

3.2.1.2. Gas Flooding Stage. Figure 14 shows the state of the fractured-vuggy network model after the gas flooding stage. As shown, after gas was injected, it only entered the top fractured-vuggy area along the first horizontal fracture due to its lower density. The gas pushed the oil horizontally through the fracture. At the end of the gas flooding stage, gas channeling occurred from the top voids, preventing further oil displacement. Oil remained in the middle of the model, occupying the vugs, and in the lower parts of the horizontal fracture in the upper vugs, in the form of oil and water. The oil−water interface shifted slightly compared to the water flooding stage.

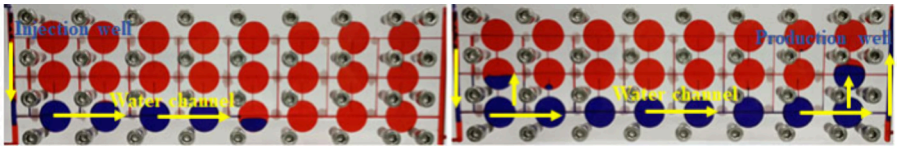

Figure 13. State of the fractured-vuggy network model after water flooding.

https://doi.org/10.1021/acsomega.4c05686
ACS Omega 2024, 9, 40810−40820

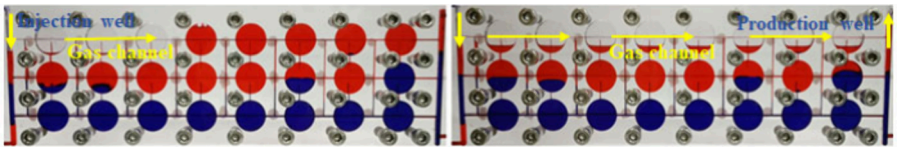

Figure 14. State of the fractured-vuggy network model after gas flooding.

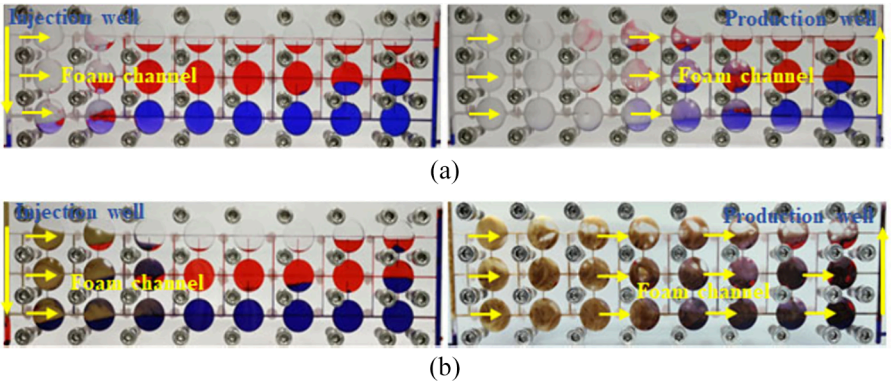

Figure 15. State of fractured-vuggy network model after foam flooding: (a) ordinary foam flooding; (b) gel foam flooding.

3.2.1.3. Foam Flooding Stage. Figure 15 shows the state of the fractured-vuggy network model after ordinary foam flooding and gel foam flooding following the gas flooding stage. As shown in Figure 15a, after foam was injected, it successively entered the three horizontal fractures from top to bottom and then into the vugs. In the middle fracture and voids, the foam displaced some oil to the right and downward along the fracture. During this process, the foam released liquid that moved through the vertical fractures into the water in the bottom vugs. While the foam could effectively displace the remaining oil near the injection well, with the deepening of foam, the increased flow distance and continuous contact with oil caused the foam to break down, thinning the liquid film and leading to gas escaping. This made it difficult for the foam to reach deeper into the reservoir, resulting in significant remaining oil near the production well. According to the calculation of the sweep area by ordinary foam, the sweep rate was 70.8%.

As shown in Figure 15b, the gel foam also entered three fractures and voids in turn after being injected. Once in the vugs, the gel foam first filled the top of the vugs and quickly occupied the entire vugs, displacing the oil and pushing the formation oil and water toward the production well. Gel foam entering the upper vugs compressed the gas, and this combined action pushed the oil in the upper vugs near the well downward, helping to displace the oil out of the horizontal fractures near the production well. Gel foam maintained its stability after contacted with oil, and its density allowed it to displace almost all the fluids in the middle and bottom regions. Only a small amount of oil remained in the vugs near the production well due to insufficient pressure gradient to push it out. The gel foam formed gel, making it difficult for subsequent fluid to mobilize this trapped oil, resulting in dynamic oil trapping. Gel foam nearly reached all the fractures and vugs, but some areas in the top vugs remain partially filled, leaving some remaining oil. The sweep rate of gel foam, based on the vugs it affected, was 91.6%.

The cumulative recovery at different stages of the two foam systems is shown in Figure 16. As seen, the cumulative

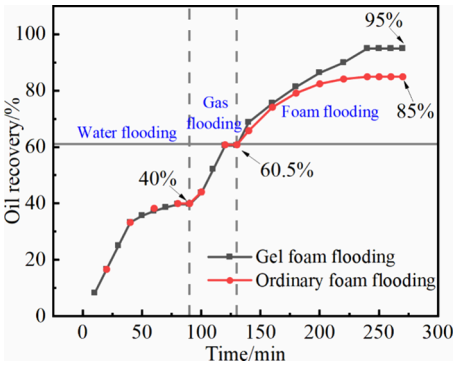

Figure 16. Cumulative oil recovery of the fractured-vuggy network model.

recovery at the end of the water flooding stage was 40%, and at the end of the gas flooding stage, it was 60.5%. After ordinary foam flooding following gas flooding, the final recovery was 85%, while the final recovery after gel foam flooding following gas flooding was 95%. There is a significant difference in the final recovery between the two foam systems. This is because gel foam's stronger stability and good viscoelasticity enable it to plug fractures and vugs effectively, control the flow direction of the top gas, and synergistically drive the recovery of the remaining oil.[31]

3.2.2. Displacement Characteristics in Fractures-Irregular Vugs Combination Model. Experiments of water flooding, gas flooding, and gel foam flooding were carried out by using fractures-irregular vugs combination model, with a fluid flow rate of 0.5 mL/min, to study the displacement effect of gel foam in a strong heterogeneous fractured-vuggy reservoir. The distribution of fluids at different displacement stages is shown in Figure 16, and the cumulative recovery at different stages is shown in Figure 17.

As seen in Figure 17a, after water injection, the water initially flowed horizontally through the bottom fractures of the model and then moved upward through the vertical fractures into vugs **c** and **d**. Once vug **c** was filled with water, water entered vug **a** from the bottom. When the oil−water

https://doi.org/10.1021/acsomega.4c05686
ACS Omega 2024, 9, 40810−40820

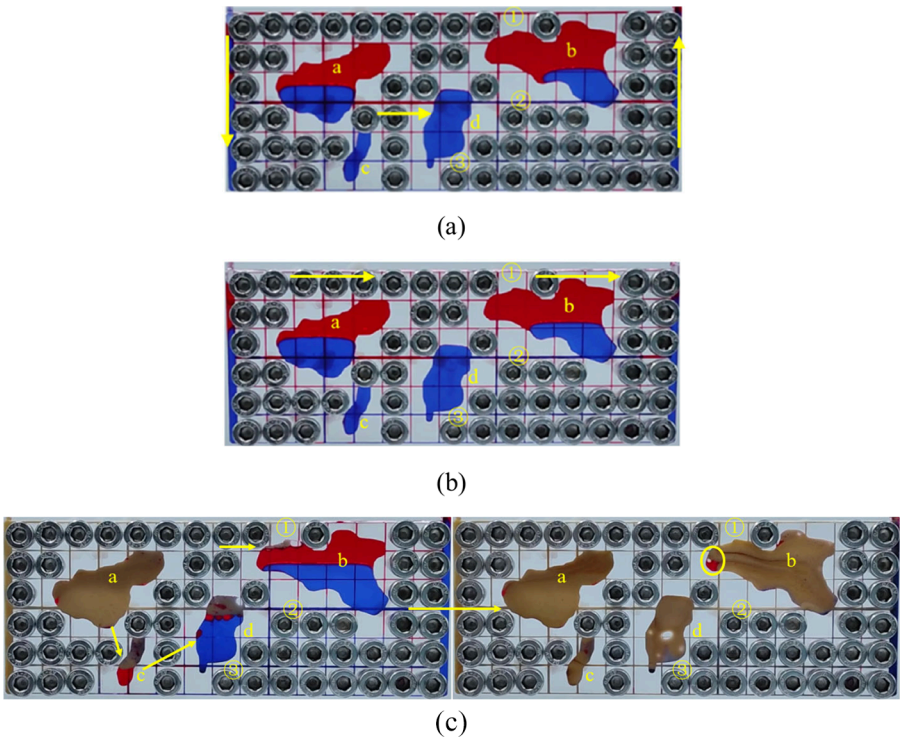

Figure 17. Fluid distribution at different displacement stages: (a) water flooding; (b) gas flooding; (c) gel foam flooding.

interface reached fracture ② with an opening of 1.2 mm in the middle of the model, this fracture became the main pathway for water flooding. Water flowed along this fracture into vug **b** and the production well, quickly leading to water channeling. After the water flooding stage, the remaining oil was primarily located at the top of vugs **a** and **b** above fracture ② and in the low-permeability fracture area in the lower right part of the model. The cumulative recovery at this stage was 45.5%.

Figure 17b shows the fluid distribution at the end of the gas flooding stage. In the model, the topmost horizontal connecting fracture ① has an opening of 0.8 mm, which is relatively high in permeability compared to the entire fracture network. After gas injection, the gas channeled along the top fracture ①, displacing only the oil in it. The sweep area was very small, and the recovery during the gas flooding stage was only 6.4%.

As shown in Figure 17c, when gel foam flooding was conducted after gas flooding, the gel foam, due to its density, pushed the remaining oil downward and to the right into voids **c** and **d**. As gel foam was continuously injected, it could displace most of the oil and plug the high-permeability channels, leaving only a small amount of remaining oil in the circled area in the figure. This is because the oil in this area is shielded by the fractures above and to the right, making it difficult for the gel foam to reach, resulting in unsweepable residual oil. As shown in Figure 18, the gel foam significantly improved the recovery, with a stage recovery rate of 48%, and the final cumulative recovery reached 93.5%.

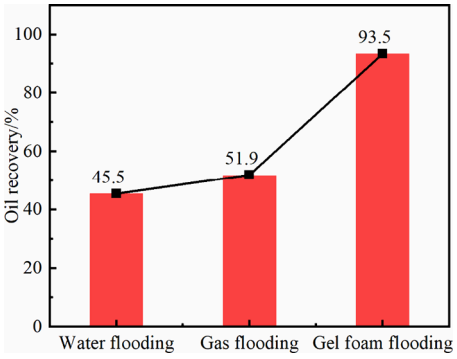

Figure 18. Cumulative oil recovery of fracture-irregular vugs combination model.

4. CONCLUSIONS

This study first investigated the plugging and flow regulation performance of gel foam in fractures by using a regular single fracture model. Further, through oil displacement experiments in typical fractured-vuggy models, the EOR effects of gel foam in different fractured-vuggy structures were clarified. This study verified the feasibility of EOR in fractured, vuggy reservoirs using gel foam.

(1) For the same fracture opening, the dynamic plugging ability of gel foam was superior to that of ordinary foam. As the fracture opening decreased, the viscoelasticity of gel foam increased the flow resistance, making the plugging effect more significant.

(2) Gel foam had strong retention ability in fractures. After large-opening fracture was plugged, the diversion rate of small-opening fracture during subsequent parallel water flooding increased by at least 83.3 times, demonstrating significant flow regulation effects.

(3) In the regular fractured-vuggy network model, after water flooding and gas flooding, the remaining oil was mainly distributed in the middle and parts of the upper vugs. Gel foam could adhere to and occupy fractures and vugs for plugging and controlled the top gas migration direction to jointly drive the remaining oil. The sweep rate of gel foam was 20.8% higher

https://doi.org/10.1021/acsomega.4c05686
ACS Omega 2024, 9, 40810−40820

than that of ordinary foam, achieving a final recovery rate of 95%.

(4) In the fractures-irregular vugs combination model, gel foam continuously advanced down and to the right along the fracture due to the density, pushing the oil and formation water in the vugs to migrate to the production well, and finally only a small amount of shielded remaining oil was difficult to drive. The recovery of gel foam flooding stage was as high as 48%, and the final recovery reached 93.5%.

AUTHOR INFORMATION

Corresponding Author

Binfei Li − *State Key Laboratory of Deep Oil and Gas, China University of Petroleum (East China), Qingdao 266580, P. R. China; School of Petroleum Engineering, China University of Petroleum (East China), Qingdao 266580, P. R. China;* orcid.org/0000-0002-8938-9731; Email: libinfei999@126.com

Authors

Yingda Yang − *Engineering Technology Research Institute, Northwest Oilfield Company, SINOPEC, Urumqi 830011, P. R. China*

Gen Rong − *Engineering Technology Research Institute, Northwest Oilfield Company, SINOPEC, Urumqi 830011, P. R. China*

Yan Xin − *State Key Laboratory of Deep Oil and Gas, China University of Petroleum (East China), Qingdao 266580, P. R. China; School of Petroleum Engineering, China University of Petroleum (East China), Qingdao 266580, P. R. China*

Yongjin Song − *State Key Laboratory of Deep Oil and Gas, China University of Petroleum (East China), Qingdao 266580, P. R. China; School of Petroleum Engineering, China University of Petroleum (East China), Qingdao 266580, P. R. China*

Complete contact information is available at: https://pubs.acs.org/10.1021/acsomega.4c05686

Author Contributions

Yingda Yang: Supervision, Resources, Writing - Review & Editing. Gen Rong: Project administration, Writing - Review & Editing. Yan Xin: Methodology, Writing-Original Draft, Writing - Review & Editing. Yongjin Song: Validation, Methodology, Data curation. Binfei Li: Investigation, Resources, Writing − Review & Editing.

Notes

The authors declare no competing financial interest.

ACKNOWLEDGMENTS

We acknowledge the Shandong Engineering Research Center of Carbon Dioxide Utilization and Storage for the assistance with our experimental research.

REFERENCES

(1) Esrafili-Dizaji, B.; Rahimpour-Bonab, H. Carbonate reservoir rocks at giant oil and gas fields in SW Iran and the adjacent offshore: a review of stratigraphic occurrence and poro-perm characteristics. *J. Pet. Geol.* **2019**, *42* (4), 343−370.

(2) Li, Y.; Kang, Z.; Xue, Z.; Zheng, S. Theories and practices of carbonate reservoirs development in China. *Pet. Explor. Dev.* **2018**, *45* (4), 712−722.

(3) Wang, X.; Zeng, L.; Wei, H.; Sun, J.; Shi, J.; Xu, X.; Cao, D.; Lu, S. Research Progress of the Fractured-vuggy Reservoir Zones in Carbonate Reservoir. *Adv. Earth Sci.* **2018**, *33* (8), 818−832.

(4) Jiao, F. Practice and knowledge of volumetric development of deep fractured-vuggy carbonate reservoirs in Tarim Basin, NW China. *Pet. Explor. Dev.* **2019**, *46* (3), 576−582.

(5) Hou, J.; Zheng, Z.; Song, Z.; Luo, M.; Li, H.; Zhang, L.; Yuan, D. Three-dimensional physical simulation and optimization of water injection of a multi-well fractured-vuggy unit. *Pet. Sci.* **2016**, *13* (2), 259−271.

(6) Qiang, J.; Yang, L.; Zhong, S.; Zou, S. Karst zonings and fracture-cave structure characteristics of Ordovician reservoirs in Tahe oilfield, Tarim Basin. *Acta Petrolei Sin.* **2016**, *37* (3), 289−298.

(7) He, J.; Li, A.; Wu, S.; Tang, R.; Lv, D.; Li, Y.; Li, X. Experimental Investigation on Injection and Production Pattern in Fractured-Vuggy Carbonate Reservoirs. *Energies.* **2020**, *13* (3), 603.

(8) Lu, G.; Zhang, L.; Liu, Q.; Xu, Q.; Zhao, Y.; Li, X.; Deng, G.; Wang, Y. Experiment analysis of remaining oil distribution and potential tapping for fractured-vuggy reservoir. *J. Pet. Sci. Eng.* **2022**, *208*, 109544.

(9) Qu, M.; Hou, J.; Wen, Y.; Liang, T. Nitrogen gas channeling characteristics in fracture-vuggy carbonate reservoirs. *J. Pet. Sci. Eng.* **2020**, *186*, 106723.

(10) Xu, Z.; Li, S.; Li, B.; Chen, D.; Liu, Z.; Li, Z. A review of development methods and EOR technologies for carbonate reservoirs. *Pet. Sci.* **2020**, *17* (4), 990−1013.

(11) Li, Y.; Fan, Z. Developmental pattern and distribution rule of the fracture-cavity system of Ordovician carbonate reservoirs in the Tahe Oilfield. *Acta Petrolei Sin.* **2011**, *32* (1), 101−106.

(12) Lyu, X.; Liu, Z.; Hou, J.; Lyu, T. Mechanism and influencing factors of EOR by N_2 injection in fractured-vuggy carbonate reservoirs. *J. Nat. Gas Sci. Eng.* **2017**, *40*, 226−235.

(13) Zheng, S.; Yang, M.; Kang, Z.; Liu, Z.; Long, X.; Liu, K.; Li, X.; Zhang, S. Controlling factors of remaining oil distribution after water flooding and enhanced oil recovery methods for fracture-cavity carbonate reservoirs in Tahe Oilfield. *Pet. Explor. Dev.* **2019**, *46* (4), 786−795.

(14) Qu, M.; Hou, J.; Qi, P.; Zhao, F.; Ma, S.; Churchwell, L.; Wang, Q.; Li, H.; Yang, T. Experimental study of fluid behaviors from water and nitrogen floods on a 3-D visual fractured-vuggy model. *J. Pet. Sci. Eng.* **2018**, *166*, 871−879.

(15) Wen, Y.; Qu, M.; Hou, J.; Liang, T.; Raj, I.; Ma, S.; Yuan, N. Experimental study on nitrogen drive and foam assisted nitrogen drive in varying-aperture fractures of carbonate reservoir. *J. Pet. Sci. Eng.* **2019**, *180*, 994−1005.

(16) Yang, J.; Hou, J.; Qu, M.; Liang, T.; Wen, Y. Experimental study the flow behaviors and mechanisms of nitrogen and foam assisted nitrogen gas flooding in 2-D visualized fractured-vuggy model. *J. Pet. Sci. Eng.* **2020**, *194*, 107501.

(17) Liang, T.; Hou, J.; Qu, M.; Song, C.; Li, J.; Tan, T.; Lu, X.; Zheng, Y. Flow behaviors of nitrogen and foams in micro-visual fracture-vuggy structures. *RSC Adv.* **2021**, *11* (45), 28169−28177.

(18) Qu, M.; Liang, T.; Hou, J. Study on Fluid Behaviors of Foam-Assisted Nitrogen Flooding on a Three-Dimensional Visualized Fracture-Vuggy Model. *Appl. Sci.* **2021**, *11* (23), 11082.

(19) Liu, Z.; Wang, Y.; Hou, J.; Luo, W.; Zheng, Z.; Qu, M.; Zhu, D. Feasibility study on foam-assisted gas flooding EOR technology in karstic oil reservoir. *J. China Univ. Pet., Ed. Nat. Sci.* **2018**, *42* (1), 113−118.

(20) Wen, Y.; Hou, J. Experimental Study on Multi-Dimensional Visualization Simulation of Gas and Gel Foam Flooding in Fractured-Vuggy Reservoirs. *Gels.* **2023**, *9* (9), 722.

(21) Xu, Z.; Li, Z.; Cui, S.; Li, B.; Chen, D.; Zhang, Q.; Zheng, L.; Husein, M. M. Flow characteristics and EOR mechanism of foam flooding in fractured vuggy reservoirs. *J. Pet. Sci. Eng.* **2022**, *211*, 110170.

(22) Fang, J.; Zhao, G.; Zhao, M.; Dai, C. New channel flow control agent for high-temperature and high-salinity fractured-vuggy carbonate reservoirs. *Energy Sources, Part A* **2021**, *43* (3), 337−348.

https://doi.org/10.1021/acsomega.4c05686
ACS Omega 2024, 9, 40810−40820

(23) Kang, W.; Jiang, H.; Yang, H.; Li, Z.; Zhou, B.; He, Y.; Sarsenbekuly, B.; Gabdullin, M. Study of nano-SiO_2 reinforced CO_2 foam for anti-gas channeling with a high temperature and high salinity reservoir. *J. Ind. Eng. Chem.* **2021**, *97*, 506−514.
(24) Liu, Q.; Liu, C.; Li, Y.; Fang, N.; Yan, X.; Dai, C.; Huang, Y.; Wu, Y. Preparation of dual network semi-solidified gelled-foam for sealing gas channeling in fractured-vuggy reservoirs. *J. Pet. Sci. Eng.* **2022**, *216*, 110687.
(25) Qu, M.; Hou, J.; Liang, T.; Raj, I.; Yang, Y.; Qi, P. Synthesis of α-starch based nanogel particles and its application for long-term stabilizing foam in high-salinity, high-temperature and crude oil environment. *J. Pet. Sci. Eng.* **2020**, *191*, 107185.
(26) Wen, Y.; Hou, J.; Qu, M.; Wu, W.; Liang, T.; Zhang, W.; Wu, W. Field Pilot Test of Micro-Dispersed Gel Foam in Fractured-Vuggy Carbonate Reservoirs. Presented at the SPE Annual Technical Conference and Exhibition, 2021; SPE-206073-MS, DOI: 10.2118/206073-MS.
(27) Lai, N.; Yuan, L.; Du, C.; Li, W.; Tang, L.; Wen, Y.; Zhang, Y. Preparation and evalution of foam gel compound channeling system for high temperature and high salt reservoir. *Spec. Petrochem.* **2020**, *37* (6), 16−23.
(28) Song, C.; Lu, X.; Hou, J.; Ma, C.; Qu, M.; Tan, T.; Guo, C. Preparation and performance evaluation of reinforced foam system with high temperature resistance and high salt tolerance in fracture-cavity. *Pet. Geol. Recovery Effic.* **2023**, *30* (5), 76−83.
(29) Li, C.; Hou, J.; Wen, Y.; Liang, T. Analysis of the Influencing Factors on the Extraction of Residual Oil through the Gel Foam Flooding of Underground Reservoirs in the Tahe Oilfield. *Gels* **2023**, *9* (10), 804.
(30) Yang, H.; Xu, Z.; Zhao, Y.; Zhang, B.; Cui, W.; Kang, W.; Qi, J.; Tang, Z.; Xu, P. A strong stability gel foam for water shutoff during oil and gas reservoir development. *Phys. Fluids* **2024**, *36* (2), 027133.
(31) Wang, Y.; Han, X.; Li, J.; Liu, R.; Wang, Q.; Huang, C.; Wang, X.; Zhang, L.; Lin, R. Review on Oil Displacement Technologies of Enhanced Oil Recovery: State-of-the-Art and Outlook. *Energy Fuels.* **2023**, *37* (4), 2539−2568.

https://doi.org/10.1021/acsomega.4c05686
ACS Omega 2024, 9, 40810−40820